Available online at www.sciencedirect.com
SCIENCE DIRECT
Journal of Molecular Catalysis A: Chemical 253 (2006) 99–106
JOURNAL OF MOLECULAR CATALYSIS A: CHEMICAL
www.elsevier.com/locate/molcata

Preparation, characterization and photocatalytic activity of novel TiO_2 nanoparticle-coated titanate nanorods

Huogen Yu, Jiaguo Yu *, Bei Cheng

State Key Laboratory of Advanced Technology for Material Synthesis and Processing, Wuhan University of Technology, Luoshi Road 122#, Wuhan 430070, PR China

Received 14 January 2006; accepted 8 March 2006
Available online 18 April 2006

Abstract

Anatase TiO_2 nanoparticles were uniformly coated on the surface of the titanate nanorods using TiF_4 and H_3BO_3 as the precursors via a simple solution route. The prepared samples were characterized with SEM, XRD, TEM, HRTEM and nitrogen adsorption–desorption isotherms and their photocatalytic activities were evaluated by photocatalytic decolorization of methyl orange aqueous solution. The effects of the precursor concentration, deposition time and deposition temperature on the morphology and phase structure of the TiO_2 nanoparticle-coated titanate nanorods were investigated. Compared with the titanate nanorods, the novel TiO_2 nanoparticle-coated titanate nanorods showed an obvious increase in the specific surface area and pore volume due to the formation of TiO_2 nanoparticles (10–50 nm) on the surface of the titanate nanorods. Moreover, the TiO_2 nanoparticle-coated titanate nanorods, which could be readily separated after photocatalytic reaction, exhibited highly photocatalytic activity for the degradation of methyl orange aqueous solution.

Keywords: TiO_2; Nanoparticles; Titanate nanorods; Coating; Photocatalytic activity

1. Introduction

Low-dimensional nanostructured materials, representing ideal building blocks for the bottom-up assembly of integrated electronic and photoelectronic devices, have attracted considerable attention recently due to their unique physical and chemical properties [1–3]. To understand their fundamental properties, from both fundamental and applied viewpoints, various low-dimensional individual nanostructures with well-controlled size, shape and chemical composition, such as zero-dimensional (0D) nanoparticles and one-dimensional (1D) nanowires, nanorods, nanobelts or nanotubes of elements, oxides, nitrides, carbides and chalcogenides, have been synthesized using various strategies and their corresponding physicochemical properties have been widely investigated [4–7]. For example, semiconductor nanowires and single-walled carbon nanotubes could be used as building blocks to fabricate a range of nanodevices including field-effect transistors and diodes [8]. However, these studies of individual nanodevices represent only an initial step for the development of nanoscale devices. It remains a great challenge to assemble these low-dimensional materials into highly integrated and hierarchically organized nanostructures. To achieve integrated nanodevices, reliable methods for efficiently assembling and integrating nanobuilding blocks into arrays or circuits should be developed [9–12]. It was reported that the size- and shape-controlled nanocrystals (0D) has been successfully fabricated and assembled into 1D and superlattice structures [13,14]. Moreover, the hierarchical assembly of 1D nanostructures into well-defined functional networks was also reported [15,16]. Unfortunately, seldom studies have been focused on the preparation of 0D/1D composite nanostructures, such as nanoparticle/nanorod nanocomposites. It should be noted that the conjunction and integration of nanoparticles (0D) and nanorods (1D) represent one of the key to bridging the "bottom-up" with the "top-down" approach in future nanotechnology.

Among various oxide semiconductor photocatalysts, TiO_2 is one of the most effective photocatalysts due to its strong oxidizing power, nontoxicity, and long-term photostability [17–20]. When TiO_2 powder is used as a photocatalyst for water

* Corresponding author. Tel.: +86 27 8788 3610; fax: +86 27 8788 3610.
E-mail address: jiaguoyu@yahoo.com (J. Yu).

1381-1169/$ – see front matter © 2006 Elsevier B.V. All rights reserved.
doi:10.1016/j.molcata.2006.03.012

purification, it shows high photocatalytic activity due to its large surface area. However, conventional powdered photocatalysts have a serious limitation—the need for post-treatment separation in a slurry system after photocatalytic reaction. Also, the nanosized powders have a strong tendency to agglomerate into larger particles, resulting in the decrease of their photocatalytic performance. Continuing efforts have been made to develop alternate methods to prepare the highly active photocatalysts, which can be readily separated after the photocatalytic reaction. In this work, anatase TiO_2 nanoparticle-coated titanate nanorods were prepared by a two-step solution-phase reaction. The first step was to prepare 1D titanate nanorods, and the second was to obtain the self-assembly of TiO_2 nanoparticles on the surface of titanate nanorods. The effects of the precursor concentration, deposition time and deposition temperature on the morphology and phase structure of the TiO_2 nanoparticle-coated titanate nanorods were investigated and discussed. The photocatalytic activities of the titanate nanorods before and after the deposition of the TiO_2 nanoparticles were evaluated by photocatalytic decolorization of methyl orange aqueous solution.

2. Experimental

2.1. Preparation of titanate nanorods

Titanate nanorods were prepared using a chemical process similar to that described by Kasuga et al. [21,22]. TiO_2 source used for the titanate nanorods was commercial-grade TiO_2 powder (P25, Degussa AG, Germany) with crystalline structure of ca. 20% rutile and ca. 80% anatase and primary particle size of ca. 30 nm. In a typical synthesis, 1.5 g of the TiO_2 powder (P25) was mixed with 140 ml of 10 M NaOH solution, followed by hydrothermal treatment of the mixture in a 200 ml Teflon-lined stainless steel autoclave at 200 °C for 48 h. After hydrothermal reaction, the precipitate was separated by filtration and washed with a 0.1 M HCl solution and distilled water until the pH value of the rinsing solution reached ca. 6.5, approaching the pH value of the distilled water. The washed samples were dried in a vacuum oven at 80 °C for 8 h.

2.2. Preparation of TiO_2 nanoparticle-coated titanate nanorods

TiF_4 and H_3BO_3 were used as the precursors for the preparation of the TiO_2 nanoparticle-coated titanate nanorods. In a typical synthesis, TiF_4 and H_3BO_3 were dissolved in distillated water, respectively. Then, the as-prepared aqueous solutions of TiF_4 and H_3BO_3 were mixed, stirred, and used as the deposition solution. The concentrations of TiF_4 were changed from 0.005 to 0.025 M and the molar ratio of TiF_4 to H_3BO_3 was fixed to 1:3. Subsequently, 0.01 g of the washed titanate nanorods were added into 50 ml of the deposition solution and then incubated at room temperature to 80 °C for 5–36 h. After the reactions, the powdered samples were filtered, rinsed with distilled water and dried in a vacuum oven at 60 °C for 8 h.

2.3. Characterization

Morphology observation was performed on a JSM-5610LV scanning electron microscope (SEM, JEOL, Japan). X-ray diffraction (XRD) patterns were obtained on a D/MAX-RB X-ray diffractometer (Rigaku, Japan) using Cu Kα irradiation at a scan rate (2θ) of $0.05^\circ\ s^{-1}$ and were used to determine the phase structure of the obtained samples. The accelerating voltage and the applied current were 15 kV and 20 mA, respectively. Transmission electron microscopy (TEM) analyses were conducted with a JEM-2010F electron microscope (JEOL, Japan), using 200-kV accelerating voltage. Nitrogen adsorption–desorption isotherms were obtained on an ASAP 2020 (Micromeritics Instruments, USA) nitrogen adsorption apparatus. All the samples were degassed at 100 °C prior to BET measurements. The Brunauer–Emmett–Teller (BET) specific surface area (S_{BET}) was determined by a multipoint BET method using the adsorption data in the relative pressure (P/P_0) range of 0.05–0.25. Desorption isotherm was used to determine the pore size distribution using the Barret–Joyner–Halender (BJH) method [23]. The nitrogen adsorption volume at the relative pressure (P/P_0) of 0.970 was used to determine the pore volume and the average pore size.

2.4. Measurement of photocatalytic activity

The evaluation of photocatalytic activity of the prepared samples for the photocatalytic decolorization of methyl orange aqueous solution was performed at ambient temperature. Experimental process was as follows: the prepared powder samples (0.02 g) were dispersed in a 25 ml methyl orange aqueous solution with a concentration of $1.53 \times 10^{-3}\ mol\ L^{-1}$ in a rectangular cell (52 mm (W) × 155 mm (L) × 30 mm (H)). A 15-W 365 nm UV lamp (Cole-Parmer Instrument Co.) was used as a light source. The average light intensity striking on the surface of the reaction solution was about $112\ \mu W\ cm^{-2}$, as measured by a UV meter (made in the photoelectric instrument factory of Beijing normal university) with the peak intensity of 365 nm. The concentration of methyl orange was determined by an UV–vis spectrophotometer (UV-2550, Shimadzu, Japan). After UV irradiation for some time, the reaction solution was filtrated to measure the concentration change of methyl orange.

3. Results and discussion

3.1. Morphology and phase structure of the as-prepared titanate nanorods and the TiO_2 nanoparticle-coated titanate nanorods

Fig. 1a shows the SEM image of dispersed nanorods with a length range from several micrometers to several tens of micrometers. A high magnification SEM image of the nanorods was shown in Fig. 1b, indicating that the diameter of the obtained nanorods was in the range of 30–300 nm. Generally, these nanorods exhibited uniform diameters over their entire lengths. Similar results were also reported in the previous studies [24]. The corresponding XRD pattern (Fig. 2a) of the as-prepared

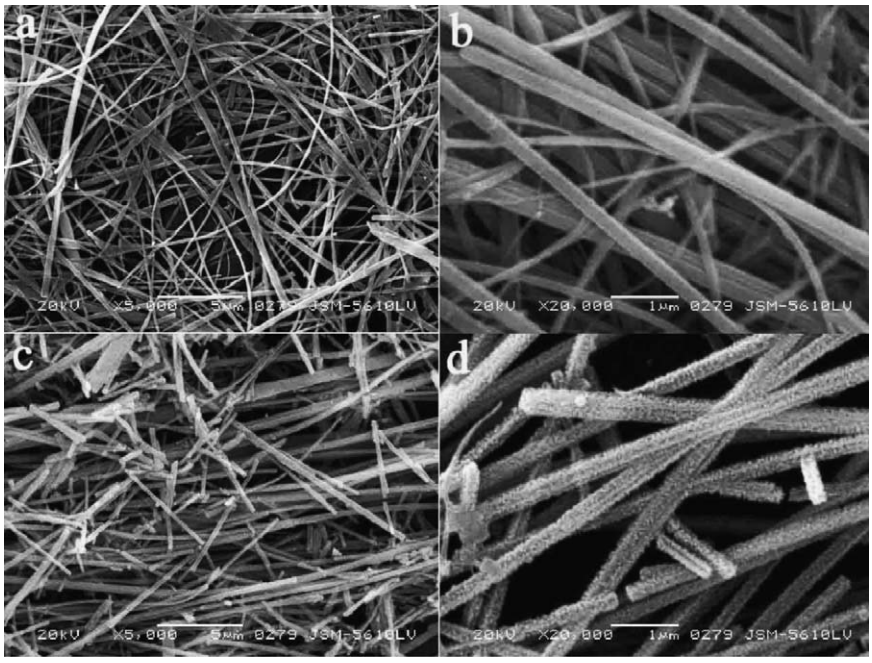

Fig. 1. SEM images of the as-prepared titanate nanorods (a and b) and the TiO_2 nanoparticle-coated titanate nanorods (c and d) obtained in a 0.01 M TiF_4 and 0.03 M H_3BO_3 mixed solution at 60 °C for 12 h.

nanorods showed a structure feature similar to that of alkali or hydrogen titanates such as $H_2Ti_3O_7$ [25], $Na_xH_{2-x}Ti_3O_7$ [26], or $Na_yH_{2-y}Ti_nO_{2n+1}\cdot xH_2O$ [27] due to a similar structure of layered titanate family.

After the washed titanate nanorods were dipped into the mixed aqueous solution of 0.01 M TiF_4 and 0.03 M H_3BO_3 and then incubated at 60 °C for 12 h, crystalline anatase TiO_2 nanoparticles could be deposited on the surface of the nanorods. The SEM image (Fig. 1c) indicates that the nanoparticles are uniformly coated on the surface of the titanate nanorods. Fig. 1d shows a high magnification SEM image, indicating that the diameter of the nanoparticles was in the range of 10–50 nm. The prepared nanoparticle-coated titanate nanorods, with uniform diameters and particle-distribution over their entire length range, are novel and should be applicable to a wide range of separation, filling, catalysis, photocatalysis. Corresponding XRD pattern (Fig. 2b) exhibited obvious diffraction peaks of anatase TiO_2 in addition to the sharp diffraction peaks of titanate, suggesting that the nanoparticles coated on the surface of the titanate nanorods were anatase TiO_2.

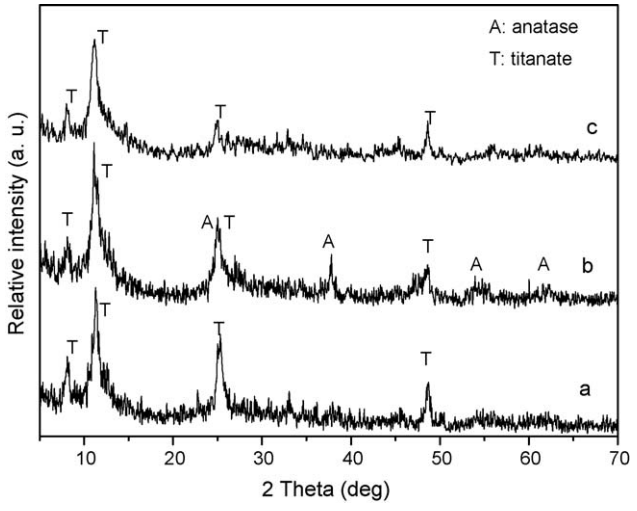

Fig. 2. XRD patterns of (a) the as-prepared titanate nanorods, (b) the TiO_2 nanoparticle-coated titanate nanorods obtained in a 0.01 M TiF_4 and 0.03 M H_3BO_3 mixed solution at 60 °C for 12 h, and (c) the TiO_2 nanoparticle-coated titanate nanorods obtained in a 0.025 M TiF_4 and 0.075 M H_3BO_3 mixed solution at room temperature for 60 h.

The morphology and microstructural details of the as-prepared titanate nanorods and the TiO_2 nanoparticle-coated titanate nanorods were further investigated by TEM analysis. Fig. 3a shows a typical TEM image of the titanate nanorods, indicating that the obtained titanate nanorods showed a wide particle size distribution of 30–300 nm. The HRTEM image indicated (Fig. 3b) that the titanate nanorods appeared an obvious layered structure, and the layer spacing was calculated to be about 0.6 nm, which was smaller than the reported value of ca. 0.8 nm [26]. This may be attributed to the dehydration among the layers of titanate nanorods during the dry of the samples in vacuum oven. After the titanate nanorods were dipped into the mixed aqueous solution of TiF_4 and H_3BO_3 and then incubated at 60 °C for 12 h, rod-like TiO_2 nanoparticles with a diameter of 10–50 nm and a length of 50–100 nm (Fig. 3c) were uniformly coated on the surface of the titanate nanorods. A high magnification TEM image (Fig. 3c, inset) indicated the formation of novel nanocomposite structures between the TiO_2 nanoparticles and the titanate nanorods. Fig. 3d shows a representative HRTEM lattice image of the TiO_2 nanoparticles coated on the surface of the titanate nanorods. By measuring the lattice fringes, the resolved interplanar distance was ca. 0.35 nm, corresponding to the (1 0 1) planes of anatase TiO_2. This also further confirmed that the crystalline structure of the

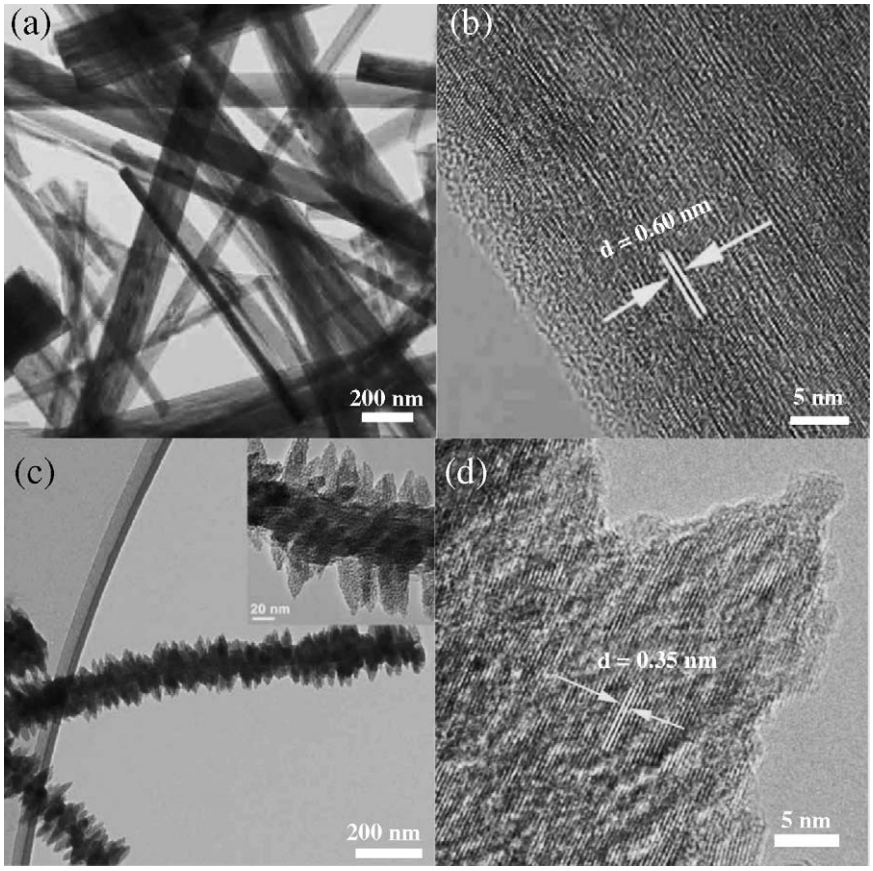

Fig. 3. TEM (a) and HRTEM images (b) of the as-prepared titanate nanorods, TEM image (c) of the TiO_2 nanoparticle-coated titanate nanorods obtained in a 0.01 M TiF_4 and 0.03 M H_3BO_3 mixed solution at 60 °C for 12 h and a high magnification TEM image (inset), HRTEM image (d) of the TiO_2 nanoparticles coated on the titanate nanorods.

TiO_2 nanoparticles coated on the titanate nanorods was anatase phase.

3.2. Preparation of TiO_2 nanoparticle-coated titanate nanorods at varying experimental conditions

For the formation of TiO_2 nanoparticles on the surface of the titanate nanorods, a formation mechanism similar to that of TiO_2 film formed on the fused quartz in our previous study was proposed [19]. A ligand exchange equilibrium reaction of metal-fluorocomplex ions and a consuming reaction of F^- ions by boric acid as F^- scavenger exist in the same reaction system as follows [19,28,29]:

$$TiF_4 + nH_2O \rightleftharpoons TiF_{4-n}(OH)n + nHF \quad (1)$$

$$H_3BO_3 + 4HF \rightleftharpoons BF_4^- + H_3O^+ + 2H_2O \quad (2)$$

H_3BO_3 was used as the F^- scavenger, which reacts readily with F^- ions to form the more stable BF_4^- ion, promoting the consumption of noncoordinated F^- ions and the formation of TiO_2 particles. Additional experimental observation showed that the solution retained a clear state during the deposition of the TiO_2 particles, indicating a low solution supersaturation. Therefore, it was deduced that the TiO_2 nanoparticles were deposited on the surface of the titanate nanorods by heterogeneous nucleation mechanism due to a lower free energy compared to homogeneous nucleation. Fig. 4a shows the SEM image of the TiO_2 nanoparticle-coated titanate nanorods obtained at a deposition time of 5 h. It was found that the TiO_2 nanoparticles with a diameter lower than 30 nm were uniformly coated on the surface of the titanate nanorods. With increasing deposition time, the TiO_2 nanoparticles showed a slow growth. After deposition for 12 h, the diameters of the TiO_2 nanoparticles coated on the titanate nanorods increased to ca. 10–50 nm. With further increase in the deposition time (36 h), the diameter of the TiO_2 nanopartilces (Fig. 4b) has no an obvious change, indicating the complete consumption of the TiF_4 precursor after deposition at 60 °C for ca. 12 h.

It was found that the concentration of TiF_4 precursor had an obvious effect on the morphology of the TiO_2 nanoparticle-coated titanate nanorods. When [TiF_4] was lower than 0.005 M, the surface of the titanate nanorods could not be completely coated by the TiO_2 nanoparticles (indicated by the arrows in Fig. 4c) due to a limited Ti species contained in the deposition solution. However, when [TiF_4] increased to 0.025 M, some spherical TiO_2 particles with a diameter of 300–500 nm (Fig. 4d) were also observed in addition to the TiO_2 nanoparticle-coated titanate nanorods. Compared with the sample obtained at [TiF_4] = 0.01 M, the TiO_2 nanoparticle-coated titanate nanorods obtained at [TiF_4] = 0.025 M showed a denser

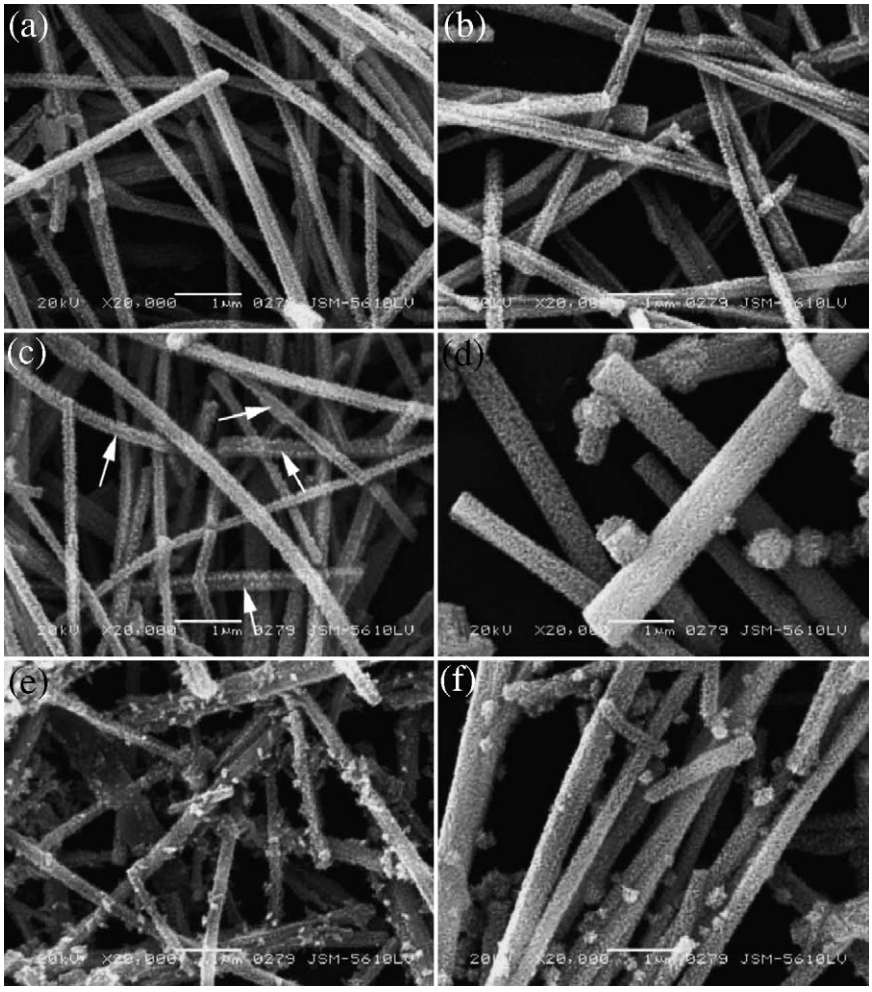

Fig. 4. SEM images of the TiO_2 nanoparticle-coated titanate nanorods obtained in (a) 0.01 M TiF_4 and 0.03 M H_3BO_3 mixed solution at 60 °C for 5 h; (b) 0.01 M TiF_4 and 0.03 M H_3BO_3 mixed solution at 60 °C for 36 h; (c) 0.005 M TiF_4 and 0.015 M H_3BO_3 mixed solution at 60 °C for 12 h; (d) 0.025 M TiF_4 and 0.075 M H_3BO_3 mixed solution at 60 °C for 12 h; (e) 0.01 M TiF_4 and 0.03 M H_3BO_3 mixed solution at 80 °C for 12 h; (f) 0.025 M TiF_4 and 0.075 M H_3BO_3 mixed solution at room temperature (ca. 20 °C) for 60 h.

surface structure. However, it was found that the concentration of TiF_4 precursor had no obvious effect on the diameter of the TiO_2 nanoparticles coated on the surface of the titanate nanorods.

Deposition temperature also had an obvious effect on the surface morphology and phase structure of the TiO_2 nanoparticle-coated titanate nanorods. When the deposition temperature increased to 80 °C, some irregular particles (Fig. 4e) were formed in addition to the TiO_2 nanoparticle-coated titanate nanorods. Further observation indicated that these irregular particles usually attached to the surface of the TiO_2 nanoparticle-coated titanate nanorods at 80 °C. This may be due to the overgrowth of some new TiO_2 nanoparticles on the surface of TiO_2 nanoparticle-coated titanate nanorods. Decreasing the deposition temperature to lower than 60 °C, the nanoparticle/nanorod composite structure similar to the sample obtained at 60 °C was also obtained even the deposition temperature was decreased to room temperature (ca. 20 °C). However, with decreasing deposition temperature, it was necessary to increase the deposition time to promote the hydrolysis of TiF_4 and the formation of TiO_2 nanoparticles due to a lower reaction rate. To decrease the deposition time, an alternative strategy was increasing the precursor concentration of TiF_4, which could accelerate the formation of TiO_2 nanoparticles on the surface of the titanate naorods. Fig. 4f shows the SEM image of the TiO_2 nanoparticle-coated titanate nanorods obtained in a 0.025 M TiF_4 and 0.075 M H_3BO_3 mixed solution at room temperature (ca. 20 °C) for 60 h. It could be seen that in addition to the TiO_2 nanoparticle-coated nanorods, some spherical TiO_2 particles composed of many smaller TiO_2 particles was also observed, similar to the result obtained at 60 °C (Fig. 4d). However, the corresponding XRD result indicated that no diffraction peaks of anatase phase were observed in addition to the diffraction peaks of the titanate nanorods, indicating that the phase structure of the TiO_2 nanoparticles coated on the titanate nanorods was amorphous TiO_2. Usually, the TiO_2 particles or films obtained by the controlled hydrolysis method at room temperature always show a weak crystallization due to the presence of impurities such as F^- ions [30]. The presence of F^- ions has been confirmed using XPS analysis (not shown here). It was reported that the existence of F^- ions could inhibit the formation of ordered titanium–oxygen networks and the crystallization of the TiO_2 films [19,30].

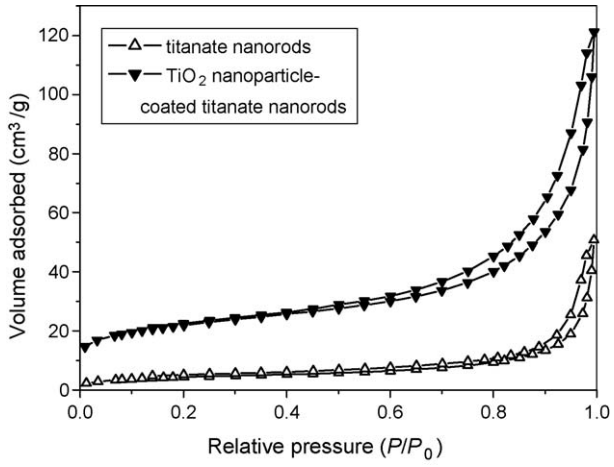

Fig. 5. Nitrogen adsorption–desorption isotherms of the titanate nanorods before and after the deposition of TiO_2 nanoparticles.

3.3. S_{BET} and pore structures of TiO_2 nanoparticle-coated titanate nanorods

The nitrogen adsorption–desorption isotherms of the titanate nanorods before and after the deposition of the TiO_2 nanoparticles are presented in Fig. 5. It can be seen that all the samples show the type IV isotherms with type H3 hysteresis loops according to BDDT calssification [23], indicating the presence of mesopores (2–50 nm). Moreover, the observed hysteresis loops of the both samples approach $P/P_0 = 1$, suggesting the presence of macropores (>50 nm) [31,32]. However, compared with the as-prepared titanate nanorods, the hysteresis loop of the TiO_2 nanoparticle-coated titanate nanorod sample shows a wider relative pressure range (0.4–1.0) and a larger area.

Fig. 6 shows the corresponding pore size distributions of the titanate nanorods before and after the deposition of the TiO_2 nanoparticles. Their textural parameters derived from the nitrogen adsorption–desorption isotherm data are summarized in Table 1. It can be seen that the pore size distributions of

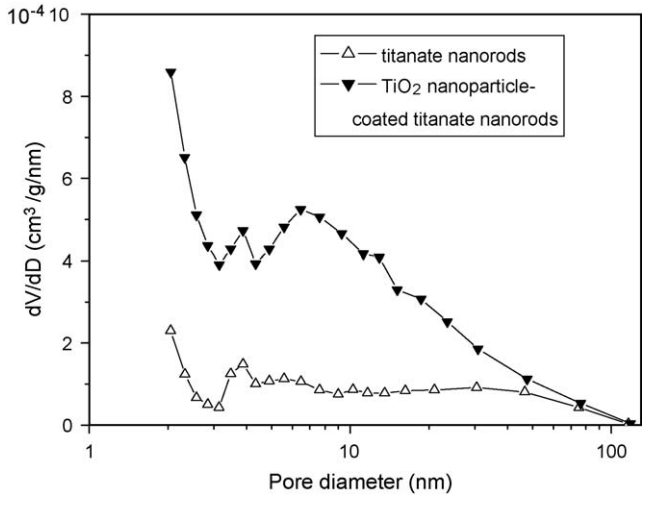

Fig. 6. Pore size distributions of the titanate nanorods before and after the deposition of TiO_2 nanoparticles.

Table 1
BET specific surface area (S_{BET}) and pore parameters of titanate nanorods before and after the deposition of TiO_2 nanoparticles

Samples	S_{BET} (m^2/g)	Pore volume (cm^3/g)	Pore size (nm)
Titanate nanorods	16.1	0.04	9.9
TiO_2 nanoparticle-coated nanorods	77.2	0.13	6.5

the titanate nanorods before and after the coating of the TiO_2 nanoparticles are obvious different. Prior to the coating of the TiO_2 nanoparticles, the titanate nanorod sample exhibits a wide pore size distribution ranging from 2 to more than 100 nm. Considering the morphology of the titanate nanorods (Fig. 3a and b), there was no mesopores and macropores existed in the individual titanate nanorods. Therefore, it was concluded that the mesopores and macropores came from the aggregations of the titanate nanrods. Owing to the absence of pores in the nanorods, the as-prepared titanate nanorods showed a small S_{BET} and pore volume, which were 16.1 m^2/g and 0.04 cm^3/g, respectively. Others also reported similar S_{BET} and pore volume of the titanate nanorods, which was 21 m^2/g for S_{BET} and 0.08 cm^3/g for pore volume [31]. After the TiO_2 nanoparticles were coated on the surface of the titanate nanorods, there was an obvious increase for S_{BET} from 16.1 to 77.2 m^2/g and for pore volume from 0.04 to 0.13 cm^3/g. On the contrary, the formation of the TiO_2 nanoparticles (10–50 nm) on the surface of the titanate nanorods resulted in the decrease of the average pore size from 9.9 to 6.5 nm (Table 1). Usually, larger specific surface area allows more reactants to be absorbed onto the surface of the photocatalyst, while higher pore volume results in a rapider diffusion of various reactants and products during the photocatalytic reaction [33].

3.4. Photocatalytic activity

The photocatalytic activities of the titanate nanorods before and after the deposition of anatase TiO_2 nanoparticles were evaluated by photocatalytic decolorization of methyl orange aqueous solution. Fig. 7 shows the plots of absorbance (A) versus irradiation time (t) for the titanate nanorods before and after the deposition of TiO_2 nanoparticles. Illumination in the absence of photocatalysts did not result in the photocatalytic decolorization of methyl orange solution. It was found that the as-prepared nanorods showed no photocatalytic activity, in contrast to the results reported by Zhu et al. [34]. In their case, the as-prepared hydrogen titanates exhibited decent photocatalytic activity for the photocatalytic oxidation of sulforhodamine (SRB) [34]. The difference in photocatalytic activity of the hydrogen titanates may be attributed to the different experimental conditions. After the anatase TiO_2 nanoparticles were uniformly coated on the surface of the titanate nanorods, the obtained sample showed highly photocatalytic activity and the concentration of the methyl orange decreased rapidly with increasing UV irradiation time. Additional experimental observation indicated that the color of the methyl orange aqueous solution changed from

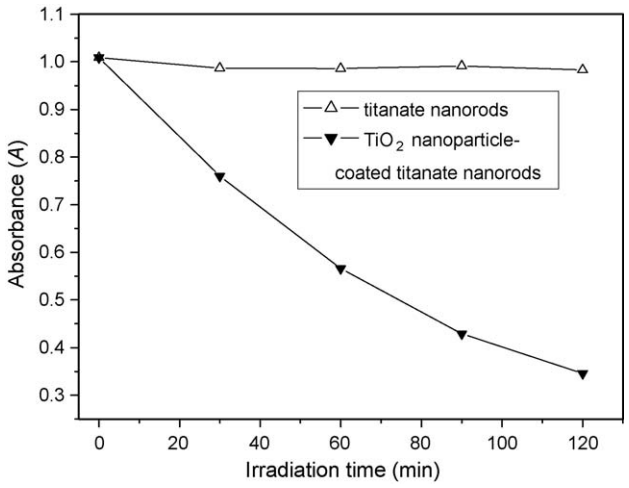

Fig. 7. Plots of absorbance (A) vs. irradiation time (t) for the titanate nanorods before and after the deposition of TiO_2 nanoparticles. Absorbance (A) in the Y-axis is proportional to the concentration (c).

orange to near no color after UV irradiation for 2 h, indicating a nearly complete degradation of methyl orange. Compared with the as-prepared titanate nanorods, the highly photocatalytic activity of the TiO_2 nanoparticle-coated titanate nanorods could be ascribed to the formation of dispersed anatase TiO_2 nanoparticles.

It is well known that TiO_2 powdered photocatalysts show a high photocatalytic activity due to their large surface area. However, powder photocatalysts have a strong tendency to agglomerate into larger particles and are difficult to be separated completely from a slurry system after photocatalytic reaction. Meanwhile, mobile powdered photocatalysts are also not applicable for air purification, as they may contribute to respirable particles that cause adverse human health problems [35]. Though this can be overcome by immobilizing TiO_2 particles as thin films on solid substrates, the formation of TiO_2 films on the substrates significantly reduces the specific surface area of TiO_2 photocatalysts, resulting in a decrease in photocatalytic activity. In this study, anatase TiO_2 nanoparticles were uniformly dotted on the surface of the nanorods with a length larger than several micrometers. Compared with the nano-sized powder photocatalysts with a particle size of several tens of nanometers, such as P25 photocatalyst, the TiO_2 nanoparticle-coated nanorod photocatalysts could be readily separated from a slurry system after photocatalytic reaction and be easily re-used owing to their mesoscale structure (usually larger than several micrometers, Fig. 1d). We think that this nanoparticle/nanorod composite structure is one of the ideal and novel photocatalysts for the applications of anatase nanoparticles in the environmental purification and treatment and would provide new insights into preparing novel highly photoactive catalysts to avoid the disadvantages of the powder and thin film photocatalysts. Therefore, the obtained TiO_2 nanoparticle-coated nanorod photocatalysts with highly photocatalytic activity may be suitable for the application of anatase photocatalysts at industrial scale, which has been seriously impeded by the high cost for separating the catalyst nanocrystals [34].

4. Conclusion

Anatase TiO_2 nanoparticles could be uniformly coated on the surface of the titanate nanorods using TiF_4 and H_3BO_3 as the precursors via a simple solution route. The precursor concentration, deposition time and deposition temperature had obvious effects on the morphology and phase structure of the TiO_2 nanoparticle-coated titanate nanorods. Compared with the titanate nanorods, the TiO_2 nanoparticle-coated titanate nanorods showed an obvious increase in the specific surface area and pore volume due to the formation of TiO_2 nanoparticles (10–50 nm) on the surface of the titanate nanorods. Moreover, the TiO_2 nanoparticle-coated titanate nanorods exhibited highly photocatalytic activity for the degradation of methyl orange aqueous solution and could be readily separated after photocatalytic reaction. This novel nanocomposite photocatalyst has potential to avoid the disadvantages of the powder and thin film photocatalysts.

Acknowledgements

This work was partially supported by the National Natural Science Foundation of China (20473059 and 50272049) and KPCME (106114). This work was also financially supported by the Excellent Young Teachers Program of MOE of China and Project-Sponsored by SRF for ROCS of SEM of China.

References

[1] Y.N. Xia, P.D. Yang, Y.G. Sun, Y.Y. Wu, B. Mayers, B. Gates, Y.D. Yin, F. Kim, Adv. Mater. 15 (2003) 353.
[2] S. Mann, W. Shenton, M. Li, S. Connolly, D. Fitzmaurice, Adv. Mater. 12 (2000) 147.
[3] Z. Tang, N.A. Kotov, Adv. Mater. 17 (2005) 951.
[4] J.G. Yu, J.C. Yu, W.K. Ho, L. Wu, X.C. Wang, J. Am. Chem. Soc. 126 (2004) 3422.
[5] T.S. Ahmadi, Z.L. Wang, T.C. Green, A. Henglein, M.A. El-Sayed, Science 272 (1996) 1924.
[6] C.M. Lieber, Solid State Commun. 107 (1998) 607.
[7] J. Hu, T.W. Odom, C.M. Lieber, Acc. Chem. Res. 32 (1999) 435.
[8] Y. Huang, C.M. Lieber, Pure Appl. Chem. 76 (2004) 2051.
[9] P.X. Gao, Z.L. Wang, J. Phys. Chem. B 106 (2002) 12653.
[10] X. Wang, J. Song, P. Li, J.H. Ryou, R.D. Dupuis, C.J. Summers, Z.L. Wang, J. Am. Chem. Soc. 127 (2005) 7920.
[11] H.G. Yang, H.C. Zeng, J. Am. Chem. Soc. 127 (2005) 270.
[12] R.S. Friedman, M.C. McAlpine, D.S. Ricketts, D. Ham, C.M. Lieber, Nature 434 (2005) 1085.
[13] Z. Tang, N.A. Kotov, M. Giersig, Science 297 (2002) 237.
[14] Z.L. Wang, S.A. Harfenist, I. Vezmar, R.L. Whetten, J. Bentley, N.D. Evans, K.B. Alexander, Adv. Mater. 10 (1998) 808.
[15] J. Hu, M. Ouyang, P. Yang, C.M. Lieber, Nature 399 (1999) 48.
[16] Y. Huang, X. Duan, Q. Wei, C.M. Lieber, Science 291 (2001) 630.
[17] M.R. Hoffmann, S.T. Martin, W. Choi, D.W. Bahnemann, Chem. Rev. 95 (1995) 69.
[18] J.C. Yu, J.G. Yu, W.K. Ho, Z.T. Jiang, L.Z. Zhang, Chem. Mater. 14 (2002) 3808.
[19] J.G. Yu, H.G. Yu, B. Cheng, X.J. Zhao, J.C. Yu, W.K. Ho, J. Phys. Chem. B 107 (2003) 13871.
[20] H.G. Yu, S.C. Lee, J.G. Yu, C.H. Ao, J. Mol. Catal. A 246 (2006) 206.
[21] T. Kasuga, M. Hiramatsu, A. Hoson, T. Sekino, K. Niihara, Langmuir 14 (1998) 3160.
[22] T. Kasuga, M. Hiramatsu, A. Hoson, T. Sekino, K. Niihara, Adv. Mater. 11 (1999) 1307.

[23] K.S.W. Sing, D.H. Everett, R.A.W. Haul, L. Moscou, R.A. Pierotti, J. Rouquerol, T. Siemieniewska, Pure Appl. Chem. 57 (1985) 603.
[24] Z.Y. Yuan, J.F. Colomer, B.L. Su, Chem. Phys. Lett. 363 (2002) 362.
[25] Q. Chen, W.Z. Zhou, G.H. Du, L.M. Peng, Adv. Mater. 14 (2002) 1208.
[26] X.M. Sun, Y.D. Li, Chem. Eur. J. 9 (2003) 2229.
[27] J. Canales, P.G. Bruce, Angew. Chem. Int. Ed. 43 (2004) 2286.
[28] C.A. Wamser, J. Am. Chem. Soc. 73 (1951) 409.
[29] H. Kishimoto, K. Takahama, N. Hashimoto, Y. Aoi, S. Deki, J. Mater. Chem. 8 (1998) 2019.
[30] T.R.N. Kutty, R. Vivekanandan, P. Murugaraj, Mater. Chem. Phys. 19 (1988) 533.
[31] D.V. Bavykin, V.N. Parmon, A.A. Lapkin, F.C. Walsh, J. Mater. Chem. 14 (2004) 3370.
[32] J.G. Yu, J.C. Yu, M.K.P. Leung, W.K. Ho, B. Cheng, X.J. Zhao, J.C. Zhao, J. Catal. 217 (2003) 69.
[33] J.G. Yu, M.H. Zhou, B. Cheng, H.G. Yu, X.J. Zhao, J. Mol. Catal. A 227 (2005) 75.
[34] H. Zhu, X. Gao, Y. Lan, D. Song, Y. Xi, J. Zhao, J. Am. Chem. Soc. 126 (2004) 8380.
[35] P.H. McMurry, Atmos. Environ. 34 (2000) 1959.